Electronic States of In_3Sb_2, In_2Sb_3, and Their Positive Ions

Ping Yi Feng[†,‡] and K. Balasubramanian*[,‡]

State Key Laboratory of Functional Materials for Informatics, Shanghai Institute of Metallurgy, Academia Sinica, Shanghai 200050, People's Republic of China, and Department of Chemistry and Biochemistry, Arizona State University, Tempe, Arizona 85287-1604

Received: June 22, 1998; In Final Form: August 14, 1998

Complete active-space multiconfiguration self-consistent field (CASSCF) followed by multireference singles + doubles configuration interaction (MRSDCI) calculations are carried out on the low-lying electronic states of In_3Sb_2, In_2Sb_3, $In_3Sb_2^+$, and $In_2Sb_3^+$. Among 8 electronic states of In_3Sb_2 considered here, 2 Jahn−Teller-distorted electronic states, $^2B_1$ (C_{2v}) and $^2A_1$ (C_{2v}), and the undistorted $^2E''$ and $^2E'$ (D_{3h}) electronic states with trigonal bipyramid geometry are close in energy. Among 5 electronic states of In_2Sb_3, a distorted edge-capped tetrahedral structure $^2B_1$ (C_{2v}) and an undistorted $^2A_2''$ (D_{3h}) are nearly degenerate. The ground states of the $In_3Sb_2^+$ and $In_2Sb_3^+$ ions are undistorted $^1A_1'$ (D_{3h}) and $^3A_2'$ (D_{3h}) states with trigonal bipyramid geometries. The singlet ($^1A_1'$)−triplet ($^3A_2'$) and singlet ($^1A_1'$)−singlet ($^1A_2'$) energy separations of the $In_3Sb_2^+$ ion are computed as 0.15 and 1.02 eV, respectively. The atomization and adiabatic ionization potentials, together with dipole moments and other properties for the electronic states of In_3Sb_2 and In_2Sb_3, are calculated and discussed. On the basis of our computed results, we also predict the ground states of $In_3Sb_2^-$ and $In_2Sb_3^-$ anions and the electron affinities of these species.

Introduction

The electronic spectroscopic, geometric, and electronic structures of mixed III−V group and other semiconductor clusters have been the topics of many investigations in recent years.[1−19] The recent proliferation of experimental studies has been made possible by the advent of several experimental techniques to generate these clusters, such as the supersonic jet expansion technique and the matrix isolation method. A motivation for such studies is that the III−V semiconductors are used in the fabrication of fast microelectronic devices. A systematic investigation of the electronic properties of the clusters could reveal how the electronic properties, geometric structures, and spectroscopic systems evolve as a function of the cluster size. Theoretical and experimental studies of clusters could provide significant insight into the properties of clusters as a function of their size and indicate the nature of low-lying electronic states of these species. There is considerable interest in learning how the properties of these clusters evolve from the cluster limit to the bulk.

Early interest in the III−V clusters arose from a pioneering work of Smalley and co-workers[1] on Ga_xAs_y, who showed that whereas the relative abundance of larger clusters followed a binomial distribution, the abundance of the smaller clusters deviated strongly from the anticipated binomial distribution. This distribution pattern has now been explained by several theoretical studies focused on the geometries and energy separations of the low-lying electronic states of these species.[13−19]

Although many of the III−V clusters have been generated in various size distributions, spectroscopic studies on these species are relatively scarce. Mandich co-workers,[11] using resonant one-color and two-color photodissociation spectroscopy, studied the stoichiometric and nonstoichiometric neutral In_xP_y clusters with $x + y$ varying from 5 to 14 atoms. They found an optical-gap-like absorption feature at the blue end of the spectra, especially for clusters with even numbers of atoms. This feature was found to be cluster-size dependent. Furthermore, odd-numbered clusters exhibited stronger and more-varied absorptions than did the even-numbered clusters. In addition, the even-numbered clusters had larger dissociation energies than the odd-numbered clusters. Thus these authors speculated that the even-numbered clusters probably have closed-shell ground states.

Weltner and co-workers[12] obtained the electron spin resonance (ESR) spectra and the hyperfine interaction of the analogous Ga_2As_3 cluster. This was accomplished by laser-heating of GaAs crystals followed by aggregation at a relatively high pressure of Ar or Kr before condensation of the matrixes at 4 K. The hyperfine structure revealed that the cluster is in a $S = {}^1/_2$ (doublet) state with a trigonal bipyramid structure.

Neumark and co-workers[6−10] studied the negative-ion photodetachment spectra of semiconductor cluster anions, particularly $In_xP_y^-$ cluster anions of various sizes. Arnold and Neumark[8] undertook a detailed spectroscopic study of the trimer clusters of the formulas In_2P and InP_2. For even-numbered In_xP_y clusters, Xu et al.[9] found an electronic gap in the spectra. These studies utilized two different spectroscopic techniques, namely, anion photoelectron spectroscopy, and anion threshold photodetachment spectroscopy, which yields zero electron kinetic energy (ZEKE) spectra, and has produced a wealth of information on the low-lying electronic states of small In_xP_y clusters and their electron affinities.

Theoretical studies of III−V semiconductor clusters have used a variety of ab initio techniques,[2,13−20] including computations on the electronic states of Ga_xAs_y clusters and, more recently, Ga_xP_y[19] ($x + y = 5$) and In_xP_y[20] ($x + y = 5$) clusters. There have been no comparable theoretical studies on In_xSb_y clusters,

* Corresponding author: fax, 602-965-2747; e-mail, KBalu@asu.edu.
† Shanghai Institute of Metallurgy.
‡ Arizona State University.

10.1021/jp982730n CCC: $15.00
Published on Web 10/10/1998

which are considerably more difficult to work with, given both the large number of electrons on In and Sb and the large relativistic effects[21,22] for the heavier Sb atoms.

The objective of this study is the first large-scale investigation of very heavy 5-atom III−V clusters, namely, In_3Sb_2, In_2Sb_3, $In_3Sb_2^+$, and $In_2Sb_3^+$. We used relativistic complete active-space multiconfiguration self-consistent field (CASSCF) followed by multireference singles + doubles configuration interaction (MRSDCI) techniques to study the low-lying electronic states of not only neutral In_3Sb_2 and In_2Sb_3 but also $In_3Sb_2^+$ and $In_2Sb_3^+$ ions. We have considered geometric optimization of several electronic states with different geometries. We have also computed the atomization energies, the adiabatic ionization energies, and the dipole moments of these clusters.

Method of Investigation

We used relativistic effective core potentials (RECPs) that retained the outer $5s^25p^3$ and $5s^25p^1$ shells for Sb and In, respectively, replacing any remaining core electrons by RECPs. The basic theoretical techniques for treating electron correlation effects and the orbitals in the current study for In_3Sb_2 and In_2Sb_3 are similar to the one we used in an earlier study on isovalent In_3P_2 and In_2P_3 clusters.[20] However, in the present study several electronic states of the positive ions of these clusters have been considered and other properties of the neutral clusters also are computed. The current description will contain only the main aspects of our calculations. A CASSCF method was used to generate the orbitals for higher-order MRSDCI computations. The RECPs and the valence Gaussian basis sets were taken from the work of Lajohn et al.[23] These basis sets were augmented with one set of 3d polarization functions on both In and Sb with exponents 0.2129 and 0.1305, respectively, as obtained from previous studies on other smaller clusters containing In and Sb.[24,25]

In our previous study[20] on the electronic states of In_3P_2 and In_2P_3, two distorted states in C_{2v} symmetry were obtained. Thus we started with geometric optimization for the low-lying electronic states of In_3Sb_2 and In_2Sb_3, using the quasi-Newton−Raphson procedure within the CASSCF level of theory. For this purpose we used the GAMESS[26] package of molecular computational codes to generate optimized geometry in C_{2v} symmetry. Two electronic states, $^2A_1$ and $^2B_1$, were found to have distorted edge-capped tetrahedral structures with C_{2v} symmetry for In_3Sb_2 and In_2Sb_3. The geometries of all possible low-lying doublet and quartet electronic states for In_3Sb_2 and doublet states of In_2Sb_3 in D_{3h} symmetry were also consequently optimized. With In_3P_2 and In_2P_3, we would expect an electronic of E′ or E″ symmetry to undergo Jahn−Teller distortion. Thus the electronic states in distorted trigonal bipyramid structures (C_{2v}) of In_3Sb_2 and In_2Sb_3 are due to Jahn−Teller distortion from the ideal D_{3h} structures.

In the CASSCF calculations we kept the 5's orbitals of In and Sb atoms inactive; that is, excitations were not allowed in the CASSCF calculations, although these orbitals were allowed to relax at the CASSCF stage as a function of geometry. Excitations from these s orbital electrons were included at the subsequent MRSDCI computations. The CASSCF wave function that included *i* a_1, *j* b_2, *k* b_1, and *l* a_2 orbitals in the complete active space is labeled *ijkl*-CAS. From the results of comparison, we adopted 3331-CAS for In_3Sb_2 and 4221-CAS for In_2Sb_3 to keep the number of configurations at the CASSCF level from being too large.

The MRSDCI computations included as reference configurations all the configurations in the CASSCF with coefficients >0.07. All possible single and double excitations of all valence electrons (including from 5s) were included in the MRSDCI. Furthermore, the multireference Davidson correction to the MRSDCI energy was calculated, and the resulting energy separations were labeled as MRSDCI+Q, which is considered to be a full-configuration interaction (CI) estimate.

TABLE 1: Geometries and Energy Separations for the Electronic States of In_3Sb_2 and In_2Sb_3, C_{2v} Structure[a]

			state	
system		unit	$^2B_1$	$^2A_1$
In_3Sb_2	$In_2-In_1-In_3$	deg	73.8	69.3
	$Sb_1-In_1-Sb_2$	deg	53.3	69.5
	$Sb_1-In_2-Sb_2$	deg	55.3	61.4
	In_1-In_2	Å	4.428	4.227
	In_2-In_3	Å	5.315	4.805
	In_1-Sb_1	Å	3.203	2.789
	In_2-Sb_1	Å	3.096	3.115
	Sb_1-Sb_2	Å	2.871	3.179
	E (CAS)	eV	0.0	0.28
	E (MRSDCI)	eV	0.0	0.19
	E (MRSDCI+Q)	eV	0.0	0.29
In_2Sb_3	$Sb_2-Sb_1-Sb_3$	deg	60.8	64.7
	$In_1-Sb_1-In_2$	deg	87.6	124.3
	$In_1-Sb_2-In_2$	deg	122.4	113.1
	Sb_1-Sb_2	Å	2.886	2.887
	Sb_2-Sb_3	Å	2.921	3.090
	Sb_1-In_1	Å	3.961	3.130
	Sb_2-In_1	Å	3.128	3.316
	In_1-In_2	Å	5.482	5.534
	E (CAS)	eV	0.0	1.39
	E (MRSDCI)	eV	0.0	1.29
	E (MRSDCI+Q)	eV	0.1	1.27

[a] The labels of all atoms are defined in Figure 1.

The electronic states of the $In_3Sb_2^+$ and $In_2Sb_3^+$ ions were considered with the objective of computing not only the adiabatic ionization energies but also the low-lying electronic states of the positive ions. Such information would be of vital use in photoionization studies of the neutral species. Three low-lying electronic states of $In_3Sb_2^+$, and four low-lying electronic states of $In_2Sb_3^+$ were computed. The singlet−triplet and singlet−singlet energy separations of the positive ions were also computed. In addition we computed as supermolecular calculations the atomization energies to dissociate In_3Sb_2 and In_2Sb_3 into indium (^2P) and antimony atoms (^4S).

The MCSCF/MRSDCI calculations were made by using a version of ALCHEMY II codes[27] is modified by one of us (K.B.)[28] to include RECPs.

Results and Discussions

Electronic States of In_3Sb_2 and $In_3Sb_2^+$. Table 1 shows the equilibrium geometries and energy separations together with dipole moments for the two electronic states $^2B_1$ and $^2A_1$ of In_3Sb_2 exhibiting C_{2v} symmetry. Figure 1 illustrates the actual geometries of the various structures obtained here for In_3Sb_2. The $^2B_1$ state in Table 1 exhibits an edge-capped tetrahedral geometry shown in Figure 1, whereas the $^2A_1$ state exhibits a distorted trigonal bipyramidal geometry, also shown in Figure 1, for the C_{2v} trigonal bipyramid geometry. Both of these structures can be envisaged as derivatives of the D_{3h} trigonal bipyramid form arising from Jahn−Teller distortion. At the highest MRSDCI and MRSDCI+Q levels of theory, as seen from Table 1, the $^2B_1$ state prevails as the ground state of In_3Sb_2, whereas the $^2A_1$ state is 0.19 and 0.29 eV higher than $^2B_1$ by these two levels of theory, respectively.

Table 2 displays the equilibrium geometries and energy separations of the undistorted D_{3h} electronic states with trigonal

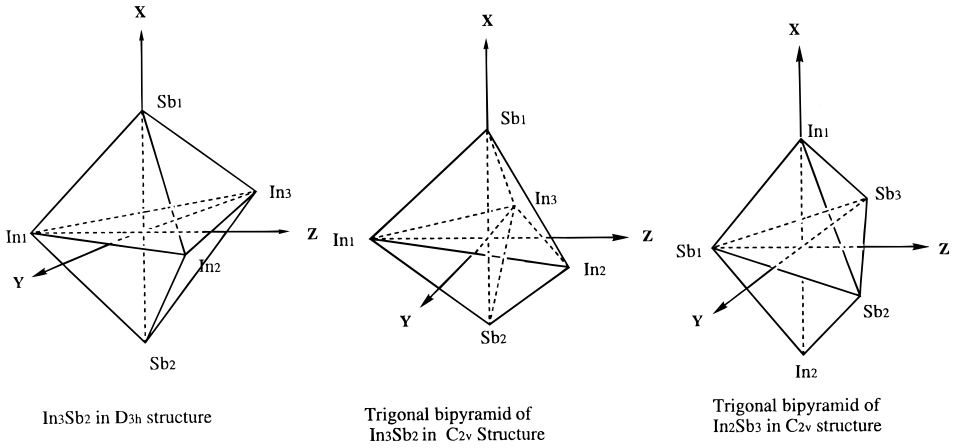

Figure 1. Geometries of the electronic states of In_3Sb_2 and In_2Sb_3 in D_{3h} and C_{2v} structures.

TABLE 2: Geometries and Energy Separations for Electronic States of In_3Sb_2 and In_2Sb_3[a]

	state		CASSCF				MRSDCI			
system	C_{2v}	D_{3h}	In−In (Å)	In−Sb (Å)	Sb−Sb (Å)	E (eV)	In−In (Å)	In−Sb (Å)	Sb−Sb (Å)	E (eV)
In_3Sb_2	$^2B_1$, $^2A_2$	$^2E''$	4.850	3.150	2.886	0.07	4.800	3.100	2.778	0.005(0.13)
	$^2A_1$, $^2B_2$	$^2E'$	4.444	3.020	3.186	0.51	4.429	3.006	3.161	0.29(0.26)
	$^4A_2$	$^4A_1''$	3.912	3.005	3.964	1.47	3.839	2.952	3.900	1.08(1.02)
	$^4B_2$	$^4A_2'$	3.317	2.939	4.459	1.68	3.287	2.911	4.415	1.11(1.14)
	$^4A_1$	$^4E'$	4.257	3.140	3.908	1.76	4.185	3.084	3.833	1.70(1.73)
	$^4B_1$	$^4E''$	3.708	3.134	4.578	1.90	3.596	3.026	4.403	8.25(8.40)
	$In_3(^4A_2) + 2Sb(^4S)$					8.09				10.12(10.42)
	$3In(^2P) + 2Sb(^4S)$					9.35				
$In_3Sb_2^+$	$^1A_1$	$^1A_1'$	4.800	3.100	2.778	6.00	4.800	3.100	2.778	6.31(6.48)
	$^3B_1$	$^3A_2''$	4.800	3.100	2.778	6.39	4.800	3.100	2.778	6.47(6.63)
	$^1B_1$	$^1A_2''$	4.800	3.100	2.778	7.49	4.800	3.100	2.778	7.42(7.50)
In_2Sb_3	C_{2v}	D_{3h}	Sb−Sb (Å)	In−Sb (Å)	In−In (Å)	E (eV)	Sb−Sb (Å)	In−Sb (Å)	In−In (Å)	E (eV)
	$^2B_1$	$^2A_2''$	2.984	2.988	4.883	0.41	2.975	2.985	4.883	0.11(0.00)
	$^2B_1$, $^2A_2$	$^2E''$	2.891	3.279	5.645	0.34	2.886	3.246	5.571	0.24(0.19)
	$^2A_1$, $^2B_2$	$^2E'$	2.953	3.257	5.550	1.49	2.949	3.232	5.494	1.36(1.31)
	$Sb_3(^2A_2) + 2In(^2P)$					6.50				6.35(5.84)
	$3Sb(^4S) + 2In(^2P)$					9.04				9.18(8.85)
$In_2Sb_3^+$	$^3B_2$	$^3A_2'$	2.886	3.246	5.571	6.13	2.886	3.246	5.571	6.39(6.40)
	$^1A_1$	$^1E'$	2.886	3.246	5.571	6.40	2.886	3.246	5.571	6.76(6.70)
	$^3B_1$	$^3A_2''$	2.886	3.246	5.571	7.54	2.886	3.246	5.571	7.67(7.61)
	$^1B_1$	$^1A_2''$	2.886	3.246	5.571	7.71	2.886	3.246	5.571	7.85(7.78)

[a] All energies are relative to the zero energy in Table 1 except the MRSDCI+Q energies (in parentheses) of In_2Sb_3.

bipyramid equilibrium geometries. As seen from Table 2, the first two low-lying electronic states of In_3Sb_2, namely, $^2E''$ and $^2E'$ states undergo Jahn−Teller distortion. The $^2B_1$ state with the edge-capped tetrahedron geometry Table 1 is one of the Jahn−Teller components of the $^2E''$ state. However, this state is only 0.05−0.13 eV above the distorted form, which suggests that the Jahn−Teller stabilization energy is very small. This picture seems to imply that, on the basis of a very small Jahn−Teller stabilization energy, the In_3Sb_2 cluster would be floppy. On the other hand, the spin−orbit effects are nonnegligible for the antimony atom and thus the $^2E''$ state would split into $E_{3/2}$ and $E_{1/2}$ spin−orbit components. We estimate the spin−orbit splitting between these two states to be 0.15 eV, based on small-scale relativistic configuration interaction (RCI) computations. Thus the spin−orbit splitting is more than the Jahn−Teller stabilization and so, by virtue of spin−orbit coupling, the $^2E''$ state of In_3Sb_2 would become a rigid D_{3h} structure.

On the basis of the computed energy separations of the excited electronic states in Table 2, and the fact that In_3Sb_2 could retain its ideal trigonal bipyramid D_{3h} structure, we predict several spectroscopic systems. As seen from Table 2, for In_3Sb_2 we compute several spectroscopic systems in the 1.02−1.73 eV region. Although the excited states are of quartet spin multiplicities, in contrast with the doublet ground states, given the spin−orbit coupling of Sb and In, we expect these electronic transitions to have nonnegligible intensities and thus these states should be observable in the spectra. Note that spectroscopic transitions are feasible from both $^2E''$ and $^2E'$ states. Furthermore, in the presence of spin−orbit coupling, the quartet and doublet electronic states would be split and mixed. For example, the $^4A_1''$ state in Table 2 would be split into $E_{3/2}$ and $E_{5/2}$ states, whereas the $^4A_2'$ state correlates into $E_{3/2}$ and $E_{5/2}$ states. The $^4E''$ and $^4E'$ states yield ($2\ E_{1/2} + E_{5/2} + E_{3/2}$) and ($E_{1/2} + 2\ E_{5/2} + E_{3/2}$), respectively. Consequently, the spin−orbit coupling could mix all states that have the same double-group-irreducible representation. Thus the spectra are likely to be perturbed by such spin−orbit mixing between different states in the D_{3h} group that have the same symmetry in the double group.

The $In_3Sb_2^+(D_{3h})$ ion exhibits three low-lying electronic states, namely, $^1A_1'$, $^3A_2''$ and $^1A_2''$, as seen from Table 2. The closed-shell ground state of $In_3Sb_2^+(D_{3h})$ can be justified on the basis of the low-lying states of the neutral In_3Sb_2, which are $^2E''$ and $^2E'$ states. Thus removal of an electron from the open-shell e″ or e′ orbital in these two states would yield the same closed-shell electronic configuration, resulting in a $^1A_1'$ state for the $In_3Sb_2^+$ ion. Consequently, the positive ion would not undergo Jahn−Teller distortion but would retain its ideal

D_{3h} structure. As seen from Table 2, the adiabatic ionization energy of In_3Sb_2 is 6.31 and 6.48 eV at the MRSDCI and MRSDCI + Q levels, respectively. Although we kept the geometry of the positive ion fixed at the neutral $^2E''$ geometry, we do not expect geometry relaxation to make a significant impact on the computed ionization energy, which should remain in a D_{3h} structure.

The excited electronic states of $In_3Sb_2^+$ can be visualized in C_{2v} symmetry as arising from the removal of the highest-occupied a_1 electron of the neutral $^2B_1$ state, which would lead to $^3B_1$ and $^1B_1$ states in C_{2v} symmetry. In D_{3h} symmetry, these states correspond to $^3A_2''$ and $^1A_2''$ states. In C_{2v} symmetry, these states are analogous to the SbH_2^+ ion,[29] which exhibits a $^1A_1$ ground state and $^3B_1$ and $^1B_1$ excited states. As seen from Table 2, the X^1A_1' to $^3A_2''$ energy separations are 0.16 and 0.15 eV at the MRSDCI and MRSDCI + Q levels, respectively. The X^1A_1' to $^1A_2''$ energy separations are 1.11 and 1.02 eV at these two levels of theory, respectively. Note that these energy separations are small and would change if the geometries of the electronic states were to be fully optimized.

Although we did not compute the properties of the electronic states of the $In_3Sb_2^-$ anion, we can, on the basis of our computed properties of the neutral In_3Sb_2 cluster and a previous computational study[25] on $InSb^-$ anion, make a few predictions about $In_3Sb_2^-$. Hotop and Lineberger[30] have listed the electron affinities (EA) of In and Sb atoms as 0.32 and 1 eV, respectively. Consequently, the two Sb atoms would primarily share the attached electron to In_3Sb_2. Attachment of an electron to the $^2E''$ or $^2E'$ state of In_3Sb_2 would result in a closed-shell $^1A_1'$ state for $In_3Sb_2^-$ with a regular trigonal bipyramid (D_{3h}) geometry. A previous theoretical study[25] yielded the second-order CI EA for InSb as 1.39 eV. Consequently, we estimate that a closed-shell $^1A_1'$ state for $In_3Sb_2^-$ should be at least 2.8 eV less than that for the neutral In_3Sb_2. This estimate is based on the fact that the negative charge will be mostly on the axial Sb atoms and that the dissociation energy of $InSb^-$ is 2.7 eV. Xu et al.[9] obtained an EA of 2.07 eV for In_3P_2. Using this EA for EA(In_3P_2), EA(Sb) = 1 eV, and EA(P) = 0.7465 eV, we estimate the EA(In_3Sb_2) to be 2.8 eV, in good agreement with the above estimate.

The nature of bonding in the electronic states can be understood through an analysis of the principal configurations, the composition of the orbitals, and the Mulliken populations. In addition, the dipole moments are computed and compared for the analysis of the ionicities of the bonds. Table 3 shows the principal configurations in the MRSDCI wave functions of the electronic states of In_3Sb_2. For the electronic states of In_3Sb_2 in C_{2v} symmetry, the ($1a_1^2 2a_1^2 3a_1^2 4a_1^2 1b_2^2 2b_2^2 1b_1^2 1a_2^2$) portion of the configuration is common for $^2B_1$ and $^2A_1$. Likewise, all the electronic states with D_{3h} structure have ($1a_1'^2 2a_1'^2 1a_2'^2 1e'^4$) in common. We describe the composition of the various molecular orbitals (MOs) in terms of the D_{3h} representation and then correlate the different MOs to C_{2v}.

The $1a_1'$ orbital ($1a_1$ in C_{2v}) is composed of Sb_1 (s) + Sb_2 (s), whereas the $2a_1'$ orbital ($2a_1$ in C_{2v}) is made of In_1 (s) + In_2 (s) + In_3 (s). The $3a_1'$ orbital ($4a_1$ in C_{2v}) is a bonding orbital with Sb_1 (s) + Sb_2 (s) and Sb_1 (p_x) + Sb_2 (p_x). The $1a_2''$ and $2a_2''$ orbitals ($1b_1$ and $3b_1$ in C_{2v}) are composed of Sb_1 (s) − Sb_2 (s) and Sb_1 (p_x) + Sb_2 (p_x), respectively, both of which are perpendicular to the In_3 plane; the two Sb atoms furnish p orbitals overlapping with opposite lobes along the *x*-axis. The two degenerate components of the 1e′ orbital ($3a_1$ and $1b_2$ in C_{2v}) are linear combinations of 2 In_1 (s) − [In_2 (s) + In_3 (s)] and In_2 (s) − In_3 (s), respectively. The two components of the 2e′ orbital ($5a_1$ and $2b_2$ in C_{2v}) are composed of 2 In_1 (s) − [In_2 (s) + In_3 (s)] + Sb_1 (p_y) + Sb_2 (p_y) and [In_2 (s) − In_3 (s)] + [Sb_1 (p_z) + Sb_2 (p_z)], respectively. The two components of the 1e″ orbital ($2b_1$ and $1a_2$ in C_{2v}) consist of In_2 (p_x) − In_3 (p_x) + Sb_1 (p_z) − Sb_2 (p_z) and In_1 (p_x) + [Sb_1 (p_y) − Sb_2 (p_y)], respectively.

TABLE 3: Leading Configurations of Electronic States of In_3Sb_2, In_2Sb_3, and Their Ions

system	state C_{2v}	state D_{3h}	coefficient	configuration[a]			
In_3Sb_2				$5a_1$	$2b_2$	$2b_1$	$1a_2$
	$^2B_1$		0.891	2	2	1	2
	$^2A_1$		0.890	1	2	2	2
				$3a_1'$	$2a_2''$	2e′	1e″
	$^2B_1$, $^2A_2$	$^2E''$	0.886	2	0	4	3
	$^2A_1$, $^2B_2$	$^2E'$	0.886	2	0	3	4
	$^4A_2$	$^4A_1''$	0.890	2	1	2	4
	$^4B_2$	$^4A_2'$	0.900	1	2	2	4
	$^4A_1$	$^4E'$	0.886	2	1	3	3
	$^4B_1$	$^4E''$	0.894	2	2	2	3
$In_3Sb_2^+$	$^1A_1$	$^1A_1'$	0.839	2	0	4	2
	$^3B_1$	$^3A_2''$	0.899	2	0	3	3
	$^1B_1$	$^1A_2''$	0.892	2	0	3	3
In_2Sb_3				$5a_1$	$2b_2$	$3b_1$	$1a_2$
	$^2B_1$		0.886	2	2	1	2
	$^2A_1$		0.892	1	2	2	2
				$3a_1'$	$2a_2''$	2e′	1e″
	$^2B_1$	$^2A_2''$	0.882	2	1	4	4
	$^2B_1$, $^2A_2$	$^2E''$	0.885	2	2	4	3
	$^2A_1$, $^2B_2$	$^2E'$	0.890	2	2	3	4
$In_2Sb_3^+$	$^3B_2$	$^3A_2'$	0.890	2	2	4	2
	$^1A_1$	$^1E'$	0.895	2	2	4	2
	$^3B_1$	$^3A_2''$	0.847	2	2	3	3
	$^1B_1$	$^1A_2''$	0.805	2	2	3	3

[a] The $1a_1^2\ 2a_1^2\ 3a_1^2\ 4a_1^2\ 1b_2^2\ 1b_1^2$ configuration part for In_3Sb_2 (or $1a_1^2\ 2a_1^2\ 3a_1^2\ 4a_1^2\ 1b_2^2\ 1b_1^2\ 2b_1^2$ for In_2Sb_3) in C_{2v} structure is same for all states. Likewise, the $1a_1'^2\ 2a_1'^2\ 1a_2''^2\ 1e'^4$ portion of the configuration for D_{3h} structure is common to all states of In_3Sb_2 and In_2Sb_3.

The geometry parameters present an interesting relationship between the various states. The bond lengths between the In atoms that form an equilateral triangle base for the $^2E''$ state are 4.80 Å at the MRSDCI level. These distances are quite close to the corresponding averaged In_1-In_2 and In_2-In_3 bond distances in the distorted $^2B_1$ state (C_{2v}), namely, 4.872 Å. However, the actual In−In bond lengths differ. On the other hand, the In−Sb bond lengths for the $^2E''$ state are 3.10 Å, which is quite close to the In−Sb bond distances of 3.15 Å in the distorted $^2B_1$ state (C_{2v}). Likewise, the Sb−Sb bond distances in the two states are 2.778 and 2.871 Å, respectively. These features suggest that Jahn−Teller distortion primarily moves the In atoms from their ideal equilateral triangular locations in In_3Sb_2. Likewise, in the $^2E'$ state, the In−In, In−Sb, and Sb−Sb bond distances are 4.429, 3.006 and 3.161 Å, respectively, close to the corresponding averaged bond lengths of 4.516, 2.952, and 3.179 Å in the $^2A_1$ distorted trigonal pyramid structure of In_3Sb_2.

The bond angles of the two distorted C_{2v} structures may also be compared. For example, the $Sb_1-In_1-Sb_2$ and $Sb_1-In_2-Sb_2$ bond angles are 53.3° and 55°, respectively, for the $^2B_1$ state. These bond angles are considerably smaller than the corresponding values of 69.3° and 61.4° for $^2A_1$, implying that the Sb−Sb bonding in $^2B_1$ is stronger than that in $^2A_1$. This is consistent with the Sb−Sb bond length in the $^2B_1$ state of 2.871 Å, which is shorter than the 3.179 Å for $^2A_1$. However, the In_1-Sb_1 bond length in $^2B_1$ (3.203 Å) is longer than that of $^2A_1$ (2.789 Å). The In_1-In_2 and In_2-In_3 bond lengths in $^2B_1$

TABLE 4: Mulliken Population Analyses for the Low-Lying Electronic States of In_3Sb_2, In_2Sb_3, and Their Ions

			gross population												
	state		total			In1			In2			Sb		
system	C_{2v}	D_{3h}	In1	In2	Sb	s	p	d	s	p	d	s	p	d
In_3Sb_2	$^2B_1$		2.520	2.548	5.692	1.876	0.617	0.027	1.862	0.656	0.031	1.942	3.576	0.173
	$^2A_1$		2.564	2.541	5.677	1.437	1.093	0.034	1.864	0.649	0.029	1.937	3.594	0.146
	$^2B_1$, $^2A_2$	$^2E''$	2.536		5.696	1.866	0.639	0.031				1.907	3.601	0.189
	$^2A_1$, $^2B_2$	$^2E'$	2.558		5.662	1.771	0.758	0.030				1.935	3.577	0.150
	$^4A_2$	$^4A_1''$	2.604		5.593	1.711	0.864	0.029				1.921	3.533	0.139
	$^4B_2$	$^4A_2'$	2.587		5.619	1.470	1.087	0.031				1.960	3.490	0.169
	$^4A_1$	$^4E'$	2.588		5.618	1.842	0.716	0.030				1.927	3.558	0.133
	$^4B_1$	$^4E''$	2.609		5.586	1.792	0.788	0.029				1.957	3.495	0.132
$In_3Sb_2^+$	$^1A_1$	$^1A_1'$	2.385		5.421	1.918	0.439	0.028				1.963	3.344	0.114
	$^3B_1$	$^3A_2''$	2.358		5.463	1.861	0.471	0.026				1.971	3.390	0.102
	$^1B_1$	$^1A_2''$	2.366		5.451	1.781	0.556	0.028				1.968	3.363	0.120
			total			Sb1			Sb2			In		
			Sb1	Sb2	In	s	p	d	s	p	d	s	p	d
In_2Sb_3	$^2B_1$		5.067	5.487	2.479	2.019	2.954	0.095	1.914	3.393	0.181	1.886	0.582	0.011
	$^2A_1$		5.449	5.310	2.465	1.987	3.289	0.173	1.997	3.155	0.158	1.866	0.585	0.016
	$^2B_1$	$^2A_2$	5.380		2.430	2.000	3.200	0.181				1.563	0.836	0.030
	$^2A_2$, $^2B_1$	$^2E''$	5.364		2.453	2.016	3.190	0.159				1.867	0.573	0.013
	$^2A_1$, $^2B_2$	$^2E'$	5.357		2.464	1.978	3.192	0.188				1.862	0.587	0.015
$In_2Sb_3^+$	$^3B_2$	$^3A_2'$	5.129		2.306	2.006	2.955	0.168				1.916	0.379	0.011
	$^1A_1$	$^1E'$	5.134		2.299	2.010	2.963	0.159				1.897	0.390	0.012
	$^3B_1$	$^3A_2''$	5.113		2.330	2.006	2.944	0.164				1.911	0.406	0.014
	$^1B_1$	$^1A_2''$	5.116		2.326	2.009	2.946	0.160				1.905	0.408	0.014

are 4.428 and 5.315 Å, respectively, both of which are longer than the corresponding bonds of $^2A_1$ (4.227 and 4.805 Å). The $In_2-In_1-In_3$ bond angle for the $^2B_1$ state (73.8°) is similar to the $In_2-In_1-In_3$ bond angle of 75.2° for the $^4A_2$ ground state in our previous study on In_3.[31]. But the In_2-In_1 bond length in the $^4A_2$ ground state for In_3 is only 2.97 Å, which is much shorter than that in In_3Sb_2. This is evidently a consequence of bonding interaction between the In and Sb atoms in the $^2B_1$ ground state of In_3Sb_2 which leads to weaker bonding between the 3 In atoms in In_3Sb_2. We conclude that the interactions between In and Sb atoms and among the Sb atoms themselves play a more-decisive role in the formation of bonds of the electronic states of In_3Sb_2. This is also consistent with the fact that the $^2B_1$ state, which exhibits enhanced Sb−Sb bonding, is more stable than $^2A_1$.

As shown in Table 2, the $^2E''$ state is the lowest among the 6 electronic states of In_3Sb_2 in D_{3h} symmetry, whereas the $^2E'$ state is immediately above the $^2E''$ state and all the quartet states are considerably well separated from the $^2E''$ state. The lowest electronic state $^2E''$ (D_{3h}) has the shortest Sb−Sb bond length (2.778 Å at the MRSDCI level) among all low-lying electronic states in D_{3h} symmetry. The Sb−Sb bond lengths in the quartet states are all >3.90 Å though they exhibit relatively contracted In−In and In−Sb bond lengths in comparison with those of the $^2E''$ state.

As evidenced from Table 3, the primary difference between the $^2B_1$ and $^2A_1$ states lies in the occupations of $5a_1$ and $2b_1$. The $5a_1$ orbital, the composition of which was described before, is a bonding orbital, it is doubly occupied in the $^2B_1$ state but singly occupied in the $^2A_1$ state. On the other hand, the $2b_1$ orbital is singly occupied in the $^2B_1$ state but fully (doubly) occupied in the $^2A_1$ state.

For the electronic states with the D_{3h} structure, the main distinction between the $^2E''$ and $^2E'$ states is in the electron occupancies for 2e′ and 1e″. All the quartet states have even fewer electrons in the 2e′ orbital than does $^2E'$. The $2a_2''$ orbital, which is perpendicular to the In_3 plane with 2 Sb atoms furnishing p orbitals with opposite lobes along the x axis, is thus antibonding with respect to Sb atoms. Thus $^2E''$ and $^2E'$ have no occupied $2a_2''$ orbital, but this orbital is singly occupied in the $^4A_1''$ and $^4E'$ states and doubly occupied in the $^4A_2'$ and $^4E''$ states. The $3a_1'$ orbital is doubly occupied by all of the electronic states except $^4A_2'$. From the above description, it is understandable that, with more occupations in the bonding orbitals, the $^2E''$ state becomes the lowest state of In_3Sb_2. A similar argument would explain the fact that the $^2E'$ state is immediately above $^2E''$, whereas all quartet states are much higher than the $^2E''$ state.

Table 4 shows the Mulliken populations of the electronic states of In_3Sb_2. As seen there, the gross populations of In are between 2.358 and 2.609 for all of the states considered here, whereas the total Sb populations are 5.421−5.696, uniformly larger than the atomic Sb populations for all of the electronic states. The s populations on Sb atoms in all the states are ≈2.0, suggesting relative inertness of the Sb $5s^2$ shell in the bond formation. This is attributed to the relativistic mass-velocity contraction of the 5s orbital of the Sb atoms.[21,22] The excess population of 0.421−0.696 on the 5p orbital of the Sb atoms is a consequence of charge transfer from the In atoms to Sb, leading to ionic In^+Sb^- bonding in In_3Sb_2.

As shown in Table 1, the $^2B_1$ (C_{2v}) state of In_3Sb_2 exhibits a positive dipole moment of 1.22 D (the positive polarity means the positive charge is on In_1 and the negative charges are on In_2 and In_3), whereas the $^2A_1$ (C_{2v}) state exhibits a negative dipole moment value of −0.62 D. This fully agrees with the Mulliken population distributions. As seen from Table 4, the gross population of In_1 (2.520) for the $^2B_1$ (C_{2v}) state is smaller than the gross populations of In_2 or In_3 (2.548). This unequal charge distribution leads to a positive dipole moment for $^2B_1$. In contrast, the total population of In_1 in the $^2A_1$ (C_{2v}) state is 2.564, which is larger than the 2.541 on In_2 or In_3 and thus results in a negative dipole moment for $^2A_1$. All the electronic states in the D_{3h} structure would exhibit zero dipole moments because of the undistorted geometries.

As also seen in Table 4, the $^2B_1$ state (C_{2v}) of In_3Sb_2 is composed of In_1 ($s^{1.876}p^{0.617}$), In_2 ($s^{1.862}p^{0.656}$), and Sb ($s^{1.942}p^{3.576}$)

Mulliken populations, (we have omitted the d population because it is <0.19). The corresponding populations for the $^2A_1$ state are In_1 ($s^{1.437}p^{1.093}$), In_2 ($s^{1.864}p^{0.649}$), and Sb ($s^{1.937}p^{3.594}$). The primary difference in the populations between these two states rests with the *s* and *p* populations on the In_1 atom. As discussed earlier, the primary difference between the two states lies in the occupations and compositions of the $5a_1$ and $2b_1$ orbitals. The $5a_1$ orbital, which has considerable $In_1(s)$ character, is fully occupied in $^2B_1$, resulting in a larger s population of 1.876 on In_1; in $^2A_1$, however, the $5a_1$ orbital is singly occupied, leading to a smaller s population of 1.437 on In_1. The $2b_1$ orbital, which contains $In_1(p_x)$, $Sb_1(p_y)$, and $Sb_2(p_y)$ contributions, is singly occupied in $^2B_1$ and doubly occupied in $^2A_1$. The full occupation of $2b_1$ consequently increases the *p* population on In for $^2A_1$, which is 1.093, whereas the *p* population on In_1 for $^2B_1$ is only 0.617. Similarly, the compositions of the 2e′ and 1e″ orbitals and the electron occupation numbers lead to larger *s* populations and smaller *p* populations on the In atoms in the $^2E''$ state (D_{3h}) in comparison with the corresponding populations in $^2E'$.

To elicit more information on the observable properties of the clusters considered here, we computed the atomization energy and adiabatic ionization energies for In_3Sb_2, obtaining the results shown in Tables 2−4. As seen from Table 2, the dissociation energy for

$$In_3Sb_2 \rightarrow In_3\ (^4A_2) + 2Sb\ (^4S)$$

is computed as 8.25 eV at the MRSDCI level by use of the previously computed ground state of $In_3(^4A_2)$.[31] We also computed the atomization energy needed to separate In_3 into 3 In atoms (^2P) as 1.87 eV at the MRSDCI level. Combining these two values, we computed the atomization energy of In_3Sb_2 that would yield 3 separated In atoms and 2 Sb atoms as 10.12 eV. These values support our conclusion that the bonding interactions between the 2 Sb atoms and the In−Sb bonds play a more important role than the In−In bonds in In_3Sb_2.

A critical comparison of the Mulliken populations of the neutral cluster and the positive ion reveals that the ionization particularly causes depletion of the charge density on the 5p orbitals rather than the 5s orbitals of In and Sb, which is consistent with the nature of the 1e″ orbital. Thus removal of a 1e″ electron decreases the *p* populations of In and Sb.

As seen from Table 2, the energy separations of the electronic states of In_3Sb_2 are very sensitive to higher-order electron correlation effects. At the CASSCF level, the $^2A_1$ (C_{2v}) state is 0.28 eV higher than the $^2B_1$ ground state of In_3Sb_2. The electron correlation effects seem to stabilize the $^2A_1$ state so that it is only 0.19 eV higher than the $^2B_1$ state at the MRSDCI level. Likewise, the undistorted $^2E'$ (D_{3h}) state is 0.51 eV above $^2E''$ at the CASSCF level, but this energy separation decreases to 0.29 eV at the MRSDCI level. The energy separations of the quartet states from $^2E''$ are 1.40−1.83 eV at the CASSCF level, whereas these values decrease to 1.06−1.65 eV at the MRSDCI level. Thus, higher-order electron correlation effects play a major role in determination of the energy separations.

Electronic States of In_2Sb_3 and $In_2Sb_3^+$. The latter half of Table 1 presents the computed properties of two electronic states of In_2Sb_3, namely, $^2B_1$ (edge-capped tetrahedron) and $^2A_1$ (distorted trigonal bipyramid) with C_{2v} symmetry, which are obtained from geometry-optimized calculations (their actual geometries shown in Figure 1). In contrast to In_3Sb_2, the $^2B_1$ state of In_2Sb_3 is lower than $^2A_1$ by 1.29 and 1.27 eV at the MRSDCI and MRSDCI + Q levels, respectively. However, as we discuss below, there are D_{3h} states quite close to the distorted structures for In_2Sb_3.

As seen from Table 2, which shows the computed properties of the undistorted trigonal bipyramid (D_{3h}) states, the $^2A_2''$ state of In_2Sb_3 is only 0.11 eV higher than the edge-capped tetrahedral $^2B_1$ state at the MRSDCI level, whereas this state becomes the ground state, with the $^2B_1$ state being 0.1 eV higher. Evidently, we can expect the spin−orbit effects to stabilize the D_{3h} structure, and the ground state of In_2Sb_3 is thus predicted to be the $^2A_2''$ state with an undistorted trigonal bipyramid D_{3h} equilibrium geometry.

We calculated all doublet electronic states of In_2Sb_3 (D_{3h}) and their optimized geometries, which are shown in the second part of Table 2 with the energy separations. As manifested in Table 2, among all doublet electronic states in D_{3h} symmetry, the $^2A_2''$ is the lowest and $^2E''$ is 0.13 eV immediately above $^2A_2''$, whereas $^2E'$ is 1.25 eV higher than $^2A_2''$ at the MRSDCI level. The $^2A_2''$ state would not undergo Jahn−Teller distortion but $^2E''$ would be subject to Jahn−Teller distortion. With Jahn−Teller stabilization, the $^2B_1$ (C_{2v}), which is a component of $^2E''$ becomes the ground state of In_2Sb_3 at the CASSCF level, but at the MRSDCI + Q level, $^2B_1$ becomes higher than the $^2A_2''$ state(D_{3h}). Interestingly, although the $^2A_2''$ state in D_{3h} symmetry has the shortest In−Sb and In−In bond lengths, the Sb−Sb bond lengths are longer among the three doublet electronic states, implying that the In−Sb bonds seem to have played a more influential role than the Sb−Sb interactions. This is consistent with the fact that, as the cluster becomes larger, the In−Sb bonds would dominate over the fewer Sb−Sb bonds.

The Jahn−Teller effect in In_2Sb_3 can be demonstrated by comparing the geometries of $^2B_1(C_{2v})$ and $^2E''$ (D_{3h}). As seen in Table 1, the 3 Sb atoms in $^2B_1(C_{2v})$ form a nearly equilateral triangle (the actual apex angle is 60.8°). The average Sb−Sb bond length (2.904 Å) of $^2B_1$ (C_{2v}) is very close to the Sb−Sb bond length (2.886 Å) of $^2E''$, suggesting little change to the 3 Sb atoms attributable to the Jahn−Teller distortion. However, the 2 In atoms move farther because of to the Jahn−Teller distortion, which results in elongated Sb_1-In_1 bonds (3.961 Å) and contracted Sb_2-In_1 bonds (3.128 Å).

The spin−orbit effects of the 3 Sb atoms could overcome the Jahn−Teller stabilization. Furthermore, at the highest level of theory (MRSDCI+Q), the $^2A_2''$ is clearly the lowest state; and thus the In_2Sb_3 cluster is expected to have an ideal D_{3h} symmetry with a trigonal bipyramid equilibrium geometry. For In_2Sb_3, we find the $^2E''$ and $^2E'$ excited states, which yield ($E_{1/2}$, $E_{3/2}$) and ($E_{3/2}$, $E_{5/2}$) spin−orbit substates,[21] respectively, while the $^2A_2''$ ground state becomes the $E_{1/2}$ state in the presence of spin−orbit coupling. Thus spectroscopic transitions from the $E_{1/2}$ ground state to $E_{1/2}$ and $E_{3/2}$ excited states of $^2E''$ and $^2E'$ (three transitions in all) should be allowed. As seen from Table 3, evidently the transition to the $E_{1/2}$ and $E_{3/2}$ spin−orbit states of the $^2E''$ state would be considerably lower in energy than the $E_{3/2}$ spin−orbit state of the $^2E'$ state. The spin−orbit splitting between $E_{1/2}$ and $E_{3/2}$ excited electronic states is estimated to be 0.2 eV bonds.

In analogy to In_2Sb_3, we can discuss the orbital compositions of the electronic states of In_3Sb_2 in D_{3h} (with the C_{2v} correlation in parentheses). The $1a_1'$ orbital ($1a_1$ in C_{2v}) is a bonding combination of Sb_1 (s) + Sb_2 (s) + Sb_3 (s), whereas the $2a_1'$ orbital ($2a_1$ in C_{2v}) is predominantly In_1 (s) + In_2 (s). The $3a_1'$ orbital ($4a_1$ in C_{2v}) is a combination of Sb_1 (s) + Sb_2 (s) + Sb_3 (s) and Sb_2 (p_y) + Sb_3 (p_y). The $1a_2''$ orbital ($1b_1$ in C_{2v}) is an antibonding combination of In_1 (s) − In_2 (s), and the $2a_2''$ orbital ($3b_1$ in C_{2v}) is predominantly made up of [In_1 (s) − In_2 (s) +

In_1 (p_x) + In_2 (p_x)] and − [Sb_1 (p_x) + Sb_2 (p_x) + Sb_3 (p_x)]. The first part represents a repulsive interaction between the 2 In atoms, whereas the second part is a π-bonding interaction between the 3 Sb atoms. The 1e′ orbital ($3a_1$ and $1b_2$ in C_{2v}) is a linear combination of 2 Sb_1 (s) − [Sb_2 (s) + Sb_3 (s)] and [Sb_2 (s) − Sb_3 (s)]. The 2e′ orbital ($5a_1$ and $2b_2$ in C_{2v}) is composed of 2Sb_1 (s) + Sb_1 (p_y) + [Sb_2 (p_z) − Sb_3 (p_z)] and [Sb_1 (p_z) + Sb_2 (p_z) + Sb_3 (p_z)] − [Sb_2 (s) + Sb_3 (s)]. The 1e″ orbital ($2b_1$ and $1a_2$ in C_{2v}) is made up of Sb_1 (p_x) − [Sb_2 (p_x) + Sb_3 (p_x)] together with [Sb_2 (p_x) − Sb_3 (p_x)], and thus contains an antibonding interaction between the 3 Sb atoms. All the electronic states in D_{3h} symmetry have ($1a_1'^2$ $2a_1'^2$ $1a_2''^2$ $1e'^4$) as a common core in their electronic configurations. The $2a_2''$ orbital is doubly occupied in all states except $^2A_2''$. The $^2E''$ state has 3 electrons in the 1e″orbital, whereas the $^2E'$ state has three electrons in the 1e′ orbital.

Table 3 exhibits the leading configurations in the MRSDCI wave functions of electronic states of In_2Sb_3. As shown, $^2B_1$ and $^2A_1$ (C_{2v}) have ($1a_1^2 2a_1^2 3a_1^2 4a_1^2 1b_2^2 1b_1^2 2b_1^2 1a_2^2$) in common. The difference between the two states from the standpoint of electronic configuration is in the occupations of $5a_1$ and $3b_1$. The $5a_1$ orbital (2e′ orbital) is bonding between Sb_1 and Sb_2 (or Sb_3) but antibonding between Sb_2 and Sb_3. Since the $5a_1$ orbital is doubly occupied in this state, it has shorter Sb_1-Sb_2 bonds (2.886 Å) along the sides and longer Sb_2-Sb_3 bonds (2.921 Å) along the base of the isosceles triangle. Meanwhile, described above, the $3b_1$ orbital consists of a repulsive interactions along the sides of the isosceles triangle of Sb_3 and at the 2 In axial atoms perpendicular to the plane of Sb_3, thus leading to longer Sb−Sb and In−In bond. This explains the higher energy of $^2A_1$, which has doubly occupied $3b_1$, than of to $^2B_1$(C_{2v}), which has only 1 electron in $3b_1$.

The $2a_2''$ orbital is doubly occupied in all states except $^2A_2''$. This orbital contains a repulsive interaction between the 2 In atoms and a π-bonding interaction between the 3 Sb atoms. Hence $^2A_2''$ (D_{3h}), with only 1 electron occupied in $2a_2''$, has longer Sb−Sb bonds and shorter In−In and In−Sb bond.

The differences in the properties of $^2E''$ and $^2E'$ arise as a consequence of the occupancies of 2e′ and 1e″ orbitals. The 2e′ orbital exhibits enhanced bonding between the 3 Sb atoms. The 1e″ orbital, on the other hand, contains an antibonding interaction between the 3 Sb atoms. With a full occupation (4 electrons) for 2e′ but less occupancy (3 electrons) for 1e″, $^2E''$ exhibits shorter Sb−Sb bonds with lower energy; the $^2E'$ state exhibits an opposite trend.

Table 4 shows Mulliken population analyses for the electronic states of In_2Sb_3. Most of the population trends discussed before for In_3Sb_2 hold for In_2Sb_3. The populations suggest In^+Sb^- polarity of bonds for all the electronic states of In_2Sb_3. The Sb (5p) populations are notably smaller than the corresponding values for In_3Sb_2. This is consistent with the fact that the charge transferred from In atoms to Sb atoms is shared by 3 Sb atoms in In_2Sb_3, whereas In_3Sb_2 the charge transfer from 3 In atoms is shared by only 2 In atoms. Thus the extent of charge transfer to each Sb atom is smaller in the case of In_2Sb_3.

As seen from Table 1, the $^2B_1$ (C_{2v}) state has a positive dipole moment; the $^2A_1$ state shows a negative one. For In_2Sb_3, the positive dipole moment means the positive charge is on Sb_1 and negative charges are on Sb_2 and Sb_3. The positive dipole moment of 1.11 D for $^2B_1$ (C_{2v}) comes from a different charge distribution on the antimony atoms, since the total population on Sb_1 (5.067) is smaller than those on Sb_2 and Sb_3 (5.487). However, the total population on Sb_1 for $^2A_1$ (5.449) is larger than those on Sb_2 and Sb_3 and thus gives a negative dipole moment of −0.45 D to $^2A_1$. All the electronic states in the D_{3h} form would have zero dipole moments because of the regular structure of that form.

As observed in Table 4, the *s* population on Sb_1 for $^2B_1$ in the C_{2v} form is larger than the corresponding population of $^2A_1$, whereas the *p* population on Sb_1 in $^2B_1$ is smaller than the corresponding population of $^2A_1$. This is fully consistent with the nature of the orbital. As pointed out earlier, the $5a_1$ orbital has enhanced Sb_1 (*s*) participation and is doubly occupied in $^2B_1$. Certainly, this would lead to a larger *s* population of Sb_1 in $^2B_1$. However, because of the double occupancy of the $3b_1$ orbital, which has enhanced 5p participation from Sb atoms, $^2A_1$ exhibits a larger 5p population on Sb. Likewise, the orbital analysis for the electronic states in D_{3h} considered before explains the larger 5s population on Sb atoms (2.016) in the $^2E''$ (D_{3h}) state than that of the $^2E'$ (1.978), but the 5p population on Sb (3.190) in $^2E''$ is slightly smaller than that of $^2E'$ (3.192).

Among all the states, $^2A_2''$ of In_2Sb_3 in D_{3h} symmetry has the smallest 5s population on In. As learned before, the $2a_2''$ orbital is mainly [In_1 (*s*) − In_2 (*s*) + In_1 (p_x) + In_2 (p_x)], which includes a contribution from the 5s of the indium atoms. The $2a_2''$ orbital is fully occupied by all the states except $^2A_2''$.

In computing the atomization energy and the adiabatic ionization energies for In_2Sb_3, we found the dissociation energy for the process

$$In_2Sb_3(^2E'') \rightarrow Sb_3(^2A_2) + 2In\ (^2P)$$

to be 6.35 eV. Combining this with the atomization energy of Sb_3 to yield 3 Sb (^4S) atoms, we obtained the atomization energy of In_2Sb_3 as 9.18 eV at the MRSDCI level. Previous theoretical studies on In_2[32] and Sb_3[33] revealed that the theoretical dissociation energy for In_2 was in good agreement with the experimental value, but for Sb_2 the calculated D_e was ∼30% smaller than the experimental value. Consequently, we expect the actual atomization energy for In_2Sb_3 to be larger than 9.18 eV.

Table 2 shows the energy separations of four electronic states of $In_2Sb_3^+$. Table 3 presents the leading configurations for the electronic states of $In_2Sb_3^+$. As shown in these tables, the calculated energy to remove a 1e″ highest occupied molecular orbital electron from $^2E''$ of the neutral In_2Sb_3 is 6.39 eV with three possible electronic states, $^3A_2'$, $^1E'$, and $^1A_1'$, formed as a result of the ionization process. However, the $^1A_1'$ state is decisively higher, being the second root of the computation in C_{2v} symmetry. Greater energy would be needed to remove an electron from 2e′ of the $^2E''$ ground state of In_2Sb_3 to lead to two excited electronic states, namely, $^3A_2''$ and $^1A_2''$. From the Mulliken population analyses shown in Table 4, there is a significant decrease in the 5p populations of the Sb atoms caused by the ionization because the removed electron comes from 1e″ or 2e′, depending on the electronic states of the positive ion, both of which have Sb (5p) as their main components. Thus, charge depletion of 5p of Sb atoms occurs in all the electronic states of $In_2Sb_3^+$.

The ground state of the $In_2Sb_3^-$ anion and the electron affinity of In_2Sb_3 can be estimated. First the ground state of the $In_2Sb_3^-$ anion is predicted to be $^1A_1'$ with regular trigonal bipyramid with D_{3h} symmetry. We expect EA(In_2Sb_3) to exceed EA(In_3Sb_2) primarily because the electron density can be shared by 3 Sb atoms, all of which have greater EA than In. Using the ratio of EA(In_3P_2) and EA(In_2P_3) obtained by Xu et al.,[9] who used anion photoelectron spectroscopy, we estimate the EA(In_2Sb_3) to be >3.7 eV.

Comparison of In_3Sb_2 and In_2Sb_3

Let us compare our computational results for In_2Sb_3 and In_3Sb_2. From Table 1, the $In_1-Sb-In_2$ angles for most of the electronic states of In_2Sb_3 become obtuse, which means that the 2 In atoms in In_2Sb_3 are widely separated. The $In_1-Sb_1-In_2$ and $In_1-Sb_2-In_2$ bond angles for the $^2B_1$ ground state of In_2Sb_3 are 87.6° and 122.4°, respectively. Evidently, the bonding between the 2 In atoms in In_2Sb_3 is very weak in contrast to In_3Sb_2, which has relatively shorter In−In bond.

A critical comparison of the Sb−Sb bond lengths in the ground states of In_2Sb_3 and In_3Sb_2 reveals that both Sb_1-Sb_2 (2.886 Å) and Sb_1-Sb_2 (2.921 Å) in the $^2B_1$ state of In_2Sb_3 are longer than the Sb_1-Sb_2 bond (2.871 Å) in $^2B_1$ for In_3Sb_2, even though there are more antimony atoms in In_2Sb_3. This reveals that the Sb−Sb interaction and not the In−Sb and In−In interactions, predominantly governs the properties of In_3Sb_2. The stronger Sb−Sb bonds result in very acute $Sb_1-In_1-Sb_2$ and $Sb_1-In_2-Sb_2$ bond angles (53.3° and 55.3°, respectively) in the ground state of In_3Sb_2. In In_2Sb_3, however, the In−Sb interactions become considerably more influential for the energy and other properties in comparison with Sb−Sb and In−In bonds. This is consistent with the longer Sb−Sb and shorter In−Sb bonds for the $^2A_2''$ state of In_2Sb_3.

The stronger Sb−Sb interaction results in enhanced dissociation energy of In_3Sb_2 into In_3 ($^4A_2$) and 2 Sb (^4S), (that is, 8.25 eV, whereas the corresponding dissociation energy of In_2Sb_3 into 2 In(^2P) + Sb_3 is 6.35 eV. Although the final atomization energy of In_3Sb_2 (10.12 eV) is slightly greater than that of In_2Sb_3 (9.18 eV), the latter value is probably less accurate since the technique underestimates the atomization energy of Sb_3. We conclude that the stabilities of In_3Sb_2 and In_2Sb_3 are quite comparable.

Although the relativistic mass-velocity stabilization of the $5s^2$ shell of the antimony atom was seen for all the electronic states of In_3Sb_2 and In_2Sb_3, there is slight difference between In_3Sb_2 and In_2Sb_3. The s populations of Sb in In_2Sb_3 are slightly larger than the corresponding values in In_3Sb_2, whereas the p populations of Sb in In_2Sb_3 are uniformly smaller than the corresponding values in In_3Sb_2, which suggests that the relativistic mass-velocity effect in In_2Sb_3 is greater than that in In_3Sb_2, as anticipated by there being more Sb atoms in In_2Sb_3. This is further supported by the fact that the relative ordering of the excited states of In_2Sb_3 changes at a higher level of theory, whereas the relative ordering of the electronic states of In_3Sb_2 does not change. This is consistent with the fact that the electron correlation effects in Sb are more than in In, so In_2Sb_3 is more influenced by electron correlation then is In_3Sb_2.

Comparison of In_3Sb_2 and In_3P_2

Given that we had previously studied[20] the electronic states of a lighter analogue, In_3P_2, we considered that a comparison of the two species might be interesting. Both of these species have two closely spaced low-lying electronic states, $^2E''$ and $^2E'$, in D_{3h} symmetry and all the quartet states are well above the lowest $^2E''$ state. Because of the increase in the atomic size as the atomic number increases within a group, we expected that the P_1-In-P_2 angle would be more acute and the In−P and P−P bond lengths of In_3P_2 shorter than to the corresponding bond angle and bond lengths in In_3Sb_2. For example, as a result of the shorter P_1-P_2 bond (2.204 Å) in the $^2B_1$ state of In_3P_2, the $P_1-In_1-P_2$ and $P_1-In_2-P_2$ bond angles are 45.2° and 47.2°, respectively.

Other notable differences exist between the two clusters. The $^2E'$ and $^4A_1'$ and $^4E''$ (D_{3h}) states in In_3P_2 are 0.40, 1.24, and 2.37 eV, respectively, greater than the $^2E''$ state, respectively. In general, 6 electronic states in In_3P_2 are more openly spaced than in In_3Sb_2, mainly because the *J*-weighted $^4S-^2D$ separation[34] for Sb is 9317 cm^{-1}, whereas the corresponding separation for P is 11 371 cm^{-1}. The Mulliken population distribution reveals other differences between the In_3P_2 and In_3Sb_2 clusters. The gross s population of Sb is almost 2.0, suggesting the inertness of the $5s^2$ shell of the antimony atom, whereas the $3s^2$ shell of the phosphorus atom is not inert (in In_3P_2 the s populations of P for the electronic states are between 1.876 and 1.905). This is consistent with considerably larger relativistic effects for Sb compared with P. The fact that only 5p orbitals of Sb participate in the bonding of In_3Sb_2 has substantial impact in the binding energies and other properties of the In_3Sb_2 cluster. All bond lengths of the electronic states of In_3P_2 are generally much shorter than the corresponding bond lengths in In_3Sb_2. For example, although the $In_2-In_1-In_3$ bond angles in the $^2B_1$ state of In_3P_2 (73.6°) and In_3Sb_2 (73.8°) are nearly the same, the In_1-In_2 and In_2-In_3 bond distances of In_3P_2 are 4.081 and 4.890 Å, respectively—much shorter than the corresponding values of In_3Sb_2 (4.428 and 5.315 Å, respectively). This suggests stronger In−In bonding interactions in In_3P_2, which, combined with the greater bond dissociation energy for the P−P bond, leads to the atomization energy of In_3P_2 being greater than that for In_3Sb_2.

Although the spectroscopic study of the In_3Sb_2 cluster apparently remains to be made, negative ion photoelectron spectroscopic studies of mixed phosphide clusters have been done.[6−10] Mandich and co-workers[11] carried out a photodissociation spectroscopic study of indium phosphide clusters composed of 5 to 14 atoms, and Xu et al.[9] obtained the electron affinities of small In_xP_y clusters ($x,y = 1-4$) by using anion photoelectron spectroscopy. Both the ground and excited states of the neutral species have been observed. In particular, the photoelectron spectrum of $In_3P_2^-$ shows two peaks very close to each other, consistent with the two nearly degenerate electronic states obtained for In_3P_2. This seems to be in accord with the two nearly degenerate low-lying electronic states of In_3Sb_2, the energy separation between these two states being only 0.13 eV at the MRSDCI+Q level of theory. Thus In_3P_2 and In_3Sb_2 are analogous in some ways, but differ in others, as noted above.

Comparison of In_2Sb_3 and In_2P_3

There are many similarities between the In_2P_3, In_2Sb_3 pairs and the In_3P_2, In_3Sb_2 pairs. Both possess the $^2E''$ and $^2E'(D_{3h})$ electronic states, which are well separated and undergo Jahn−Teller distortion to yield $^2B_1$ and $^2A_1$ states in C_{2v} symmetry. Because of the strong interaction among the 3 P atoms and weaker bonding between the 2 In atoms, the In_1-P-In_2 bond angles are almost obtuse. The $In_1-P_1-In_2$ and $In_1-P_2-In_2$ bond angles for the $^2B_1$ state of In_2P_3 are 95.1° and 128.3°, respectively. The most striking difference between In_2P_3 and In_2Sb_3 is in the ordering of states. The lowest state of In_2P_3 in the D_{3h} structure is $^2E''$, while $^2A_2''$ and $^2E'$ are 0.40 and 1.72 eV, respectively, above the $^2E''$ state at the MRSDCI level. Although this ordering is maintained at all levels of the theory for In_2P_3, larger electron correlation effects in In_2Sb_3 change the order of the $^2A_2''$ state relative to $^2E'$. Moreover, the energy separations in In_2Sb_3 are generally smaller than those in In_2P_3. As mentioned before, this is due to the small *J*-weighted $^4S-^2D$ separation.

From the Mulliken population analysis, we inferred that the s populations of P are 1.867−1.905, indicating the involvement

of 3s orbitals of P in the bonding of In_2P_3, whereas the gross *s* population of Sb is almost 2.0, implying the inertness of the $5s^2$ shell of the antimony atoms, which is attributed to the mass-velocity relativistic effect. Thus both the P−P and In−P bonds in In_2P_3 would be stronger than the Sb−Sb and In−Sb bonds in In_2Sb_3. Accordingly, the atomization energy of In_2P_3 is greater than in In_2Sb_3 because of the stronger P−P and In−P bonds in In_2P_3.

Van Zee et al.[12] investigated the matrix-isolated ESR spectra of Ga_2As_3 in Ar and Kr matrixes. Comparing their results with those for the isovalent In_2Sb_3 computed here is of interest. The matrix ESR spectra suggested that Ga_2As_3 is in a doublet spin state with a hyperfine structure consistent with 3 equivalent As atoms arranged in a regular trigonal bipyramidal structure. This is in accord with our picture for In_2Sb_3 at the MRSDCI+Q level of theory, which predicts the lowest state to be $^2A_2''$ with an ideal D_{3h} structure. However, their findings differ from ours for In_2P_3, which exhibits a $^2B_1$ ground state in a distorted trigonal bipyramidal form in C_{2v} symmetry, even though the D_{3h} state is quite close in energy. Thus, we expect there is some similarity between Ga_2As_3 and In_2Sb_3, but In_2P_3 differs from Ga_2As_3 in this aspect.

The observed spectrum of Xu et al.[9] for $In_2P_3^-$ exhibits two closely spaced peaks, which may correlate with $^2E''$ and $^2A_2''$. We have found that the lowest state of In_2Sb_3 in D_{3h} structure is $^2A_2''$, but $^2E''$ is only 0.13 eV above $^2A_2''$ at the MRSDCI level. Thus the picture for In_2P_3 is probably similar to In_2Sb_3.

Acknowledgment. This research was supported by the US National Science Foundation.

References and Notes

(1) O'Brien, S. C.; Liu, Y.; Zhang, Q. L.; Heath, J. R.; Tittel, F. K.; Curl, R. F.; Smalley, R. E. *J. Chem. Phys.* 1986, *84*, 4074. Liu, Y.; Zhang, Q. L.; Tittel, F. K.; Curl, R. F.; Smalley, R. E. *J. Chem. Phys.* **1986**, *85*, 7434.

(2) Wang, L.; Chibante, L. P. F.; Tittel, F. K.; Curl, R. F.; Smalley, R. E. *Chem. Phys. Lett.* **1990**, *172*, 335. Lou, L.; Wang, L.; Chibante, P. F.; Laaksonen, R. T.; Nordlander, P. *J. Chem. Phys.* **1991**, *94*, 8015. Lou, L.; Nordlander, P.; Smalley, R. E. *J. Chem. Phys.* **1992**, *97*, 1858.

(3) Jin, C.; Taylor, K.; Conciecao, J.; Smalley, R. E. *Chem. Phys. Lett*. **1990**, *175*, 17.

(4) Lemire, G. W.; Bishea, G. A.; Heidecke, S. A.; Morse, M. D. *J. Chem. Phys.* **1990**, *92*, 121.

(5) Lou, L.; Wang, L.; Chibante, L. P. F.; Laaksonen, R. T.; Nordlander, P.; Smalley, R. E. *J. Chem. Phys*. **1991**, *94*, 8015.

(6) Arnold, C. C.; Neumark, D. M. *J. Chem. Phys*. **1994**, *99*, 3353.

(7) Arnold, C. C.; Neumark, D. M. *J. Chem. Phys.* **1994**, *100*, 1797.

(8) Arnold, C. C.; Neumark, D. M. *Can. J. Phys*. **1994**, *72*, 1322.

(9) Xu, D.; deBeer, E.; Arnold, D. W.; Neumark, D. M. *J. Chem. Phys.* **1994**, *101*, 5406.

(10) Burton, G. R.; Xu, D.; Arnold, C. C.; Neumark, D. M. *J. Chem. Phys.* **1996**, *104*, 2757.

(11) Kolenbrander, K. D.; Mandich, M. L. *J. Chem. Phys*. **1990**, *92*, 4759. Rinnen, K.-D.; Kolenbrander, K. D.; DeSantolo, A. M.; Mandich, M. L. *J. Chem. Phys.* **1992**, *96*, 4088.

(12) VanZee, R. J.; Li, S.; Weltner, W., Jr. *J. Chem. Phys*. **1993**, *98*. 4335.

(13) Balasubramanian, K. *Chem. Phys. Lett*. **1988**, *150*, 71.

(14) Balasubramanian, K. *Chem. Rev*. **1990**, *90*, 93; *Chem. Rev.* **1989**, *89*, 1801*; J. Phys. Chem.* **1986**, *85*, 3401; *J. Chem. Phys*. **1987**, *87*, 3518.

(15) Al-Laham, M. A.; Raghavachari, K. *Chem. Phys. Lett*. **1991**, *187*, 13.

(16) Meier, U.; Peyerimhoff, S. D.; Grien, F. *Chem. Phys.* **1991**, *150*, 331.

(17) Grev, R. S.; Schaefer, H. F., III *Chem. Phys. Lett*. **1987**, *135*, 287. Raghavachari, K.; Rohlfing, C. M. *J. Chem. Phys.* **1988**, *89*, 2219.

(18) Liao, M. Z.; Dai, D.; Balasubramanian, K. *Chem. Phys. Lett*. **1995**, *239*, 124.

(19) Feng, P. Y.; Balasubramanian, K. *Chem. Phys. Lett.* **1997**, *265*, 547.

(20) Feng, P. Y.; Balasubramanian, K. *Chem. Phys. Lett.* **1998**, *283*, 167.

(21) Balasubramanian, K. *Relativistic effects in chemistry: Part A. Theory & techniques*; Wiley-Interscience: New York, 1997; p 301.

(22) Balasubramanian, K. *Relativistic effects in chemistry: Part B. Applications to molecules & clusters*; Wiley-Interscience: New York, 1997; p 527.

(23) Lajohn, L. A.; Christiansen, P. A.; Ross, R. B.; Atashroo, T.; Ermler, W. C. *J. Chem. Phys.* **1987**, *87*, 2812.

(24) Balasubramanian, K. *J. Chem. Phys.* **1990**, *93*, 507.

(25) Das, K. K.; Balasubramanian, K. *J. Chem. Phys.* **1991**, *94*, 6420.

(26) Schmidt, M. W.; Baldridge, K. K.; Boatz, J. A.; Elbert, S. T.; Gorden, M. S.; Jensen, J. H.; Koseki, S.; Matsunaga, N.; Nguyen, K. A.; Su, S. J.; Windus, T. L.; Dupuis, M.; Montgomery, J. A. *J. Comput. Chem.* **1993**, *14*, 1347.

(27) The major authors of ALHEMY II are Liu, B.; Lensfield, B.; Yoshimine, M.

(28) Balasubramanian, K. *Chem. Phys. Lett.* **1986**, *127*, 324.

(29) Balasubramanian, K. *J. Chem. Phys.* **1989**, *91*, 2443.

(30) Hotop, H.; Lineberger, W. C. *J. Phys. Chem. Ref. Data* **1985**, *14*, 731.

(31) Feng, P. Y.; Balasubramanian, K. *Chem. Phys.* **1989**, *138*, 89.

(32) Balasubramanian, K.; Li, J. Q. *Chem. Phys.* **1989**, *88*, 4979.

(33) Balasubramanian, K.; Sumathi, K.; Dai, D. *J. Chem. Phys.* **1991**, *95*, 3494.

(34) Moore, C. E. *Tables of atomic energy levels*; US National Institute of Standards and Technology: Gaithersburg, MD, 1971, Vol. I−III, Circular 467.